Stray-Capacitance As a Simple Tool for Monitoring and Locating Heat Generation Demonstrated in Three Superconducting Magnets

Daniel Davis, Tengming Shen, Maxim Marchevsky, and Emmanuele Ravaioli

***Abstract*—Real-time monitoring of heat loads in cryogenic systems is critical for many applications, particularly high field magnets. We demonstrated that by monitoring changes in the capacitance of local probes consisting of thin metal strips with a porous glass fiber dielectric, boiling helium from as little as 0.1 J of deposited heat can be located by an analysis of the response speed and amplitude in nearby probes. We further implemented stray-capacitance monitoring of a magnet's metal support structures, a more global probe of the magnet volumes, in three high temperature superconducting Bi-2212 magnet types. Global structural stray-capacitance monitoring was evaluated for a single racetrack coil, a common coil dipole, and a canted cosine theta winding, showing a quench response comparable to voltage signals without inductive effects. The response of the local and global probes was compared in the single racetrack coil with well-known quench properties. Monitoring the cool-down of the common coil dipole demonstrated the added benefit of the global stray-capacitance as a liquid level monitor. This simple method of monitoring the capacitance has proven to be a versatile and robust technique for monitoring and locating heat.**

***Index Terms*—Bi-2212, high temperature superconducting (HTS), quench, superconducting magnet.**

I. Introduction

QUICKLY detecting and locating heat sources in cryogenic systems can often prevent damage, conserve cryogens, and help diagnose problems in real time. This is particularly true for high field superconducting magnets, where heat drives the conductor to the resistive state. Traditional heat detection methods in superconducting magnets rely on voltage monitoring of the coil resistance or oxide resistor thermometers in contact with the cold mass of the magnet. Thermometer responses have delays and voltage monitoring, while often fast, can be easily compromised by inductive signals. In high temperature superconducting (HTS) magnets, early detection of heat can avoid thermal runaway, or quench, by allowing the transport current to be reduced in a reasonable amount of time before temperature limits, usually 300 K, are exceeded. At higher temperatures, coil damage rapidly becomes more likely, especially for the slow normal zone propagation of HTS coils. Higher field magnets reaching 20 T–40 T are being sought after that will require HTS. At the same time, low temperature superconducting accelerator subscale magnets for future accelerators are limited by progressive quench training challenges. Novel diagnostics that can provide information about quench dynamics and location are being sought after [1]. This has resulted in rapid implementation of techniques such as diffuse ultrasound and quench antenna [2], [3]. Further development of the stray-capacitance technique could make it a complementary diagnostic tool for understanding the sources of training. Sensitive heat detection and localization are becoming increasingly important to advancing magnet technology for both condensed matter scientists and the accelerator community.

A. Stray-Capacitance Monitoring

A simple method of quickly detecting heat generation through changes of stray-capacitance has been demonstrated within subscale HTS coils [4]–[6]. In general, any adjacent and electrically isolated metal structures can be treated as a capacitor. When this is unintended and we measure the dynamic voltage response between the isolated structures, we label the resulting stray-capacitance. As there are multiple isolated structures in a superconducting magnet, each has some stray-capacitance against the others nearby, as represented in the schematic Fig. 1. Alternatively, dedicated diagnostic sensors in the form of parallel plate capacitors, with classical capacitance, can be incorporated into key locations. Multiple factors affect the capacitance measured across structures and sensors. Capacitance will change if distances between structure surfaces change or if the dielectric properties are modified. When even small amounts of heat are

Manuscript received December 21, 2020; revised April 30, 2021 and June 20, 2021; accepted June 28, 2021. Date of publication July 7, 2021; date of current version July 30, 2021. This work at LBNL was supported by the Director, Office of Science of the U.S. Department of Energy (DOE) under Contract DE-AC02-05CH11231. The work of D. Davis was supported by the National High Magnetic Field Laboratory's National Science Foundation under Award DMR-1 157 490, the State of Florida, the U.S. DOE High Energy Physics under Award DE-SC0010421, and the U.S. DOE Office of Science Graduate Student Research (SCGSR) program, administered by ORISE and ORAU under Contract DE-SC0014664. The experimental work was performed at LBNL where D. Davis was a visiting student supported by the SCGSR program. This article was recommended by Associate Editor T. Salmi. *(Corresponding author: Daniel Davis.)*

Daniel Davis is with the National High Magnetic Field Laboratory, Tallahassee, FL 32310 USA (e-mail: ddavis@asc.magnet.fsu.edu).

Tengming Shen and Maxim Marchevsky are with the Lawrence Berkeley National Laboratory, Berkeley, CA 94720 USA (e-mail: tshen@lbl.gov; MMartchevskii@lbl.gov).

Emmanuele Ravaioli is with the CERN, 1211 Geneve, Switzerland (e-mail: Emmanuele.Ravaioli@cern.ch).

Color versions of one or more figures in this article are available at https://doi.org/10.1109/TASC.2021.3094769.

Digital Object Identifier 10.1109/TASC.2021.3094769

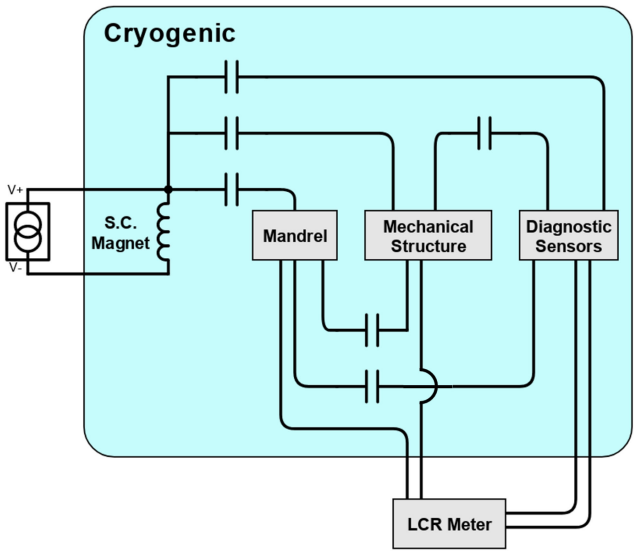

Fig. 1. Generalized circuit representation of stray-capacitance monitoring for a superconducting magnet system.

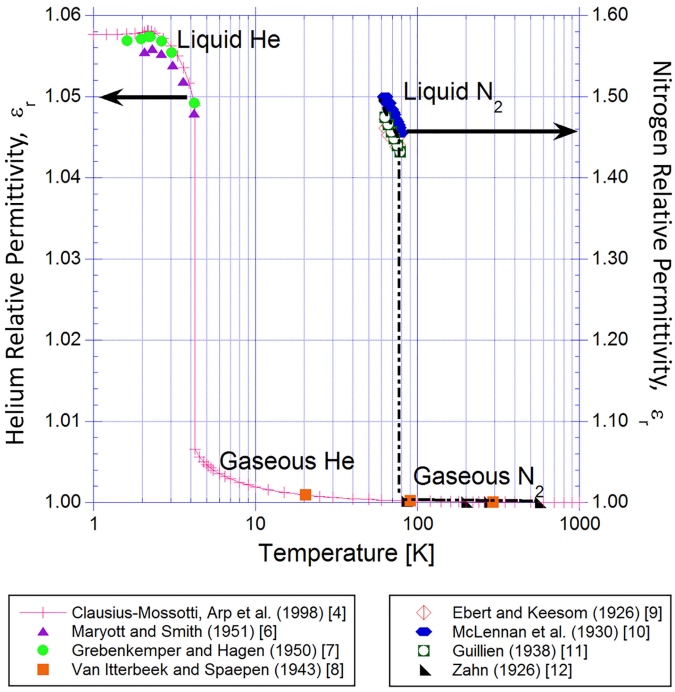

Fig. 2. Dielectric permittivity ε_r of helium (left) and nitrogen (right) as a function of temperature at atmospheric pressure showing a shift from the liquid to gaseous form [14]–[22]. Figure reproduced from [6].

generated in a liquid cryogen bath cooled system a volume of the cryogen can boil, and due to an abrupt change in the permittivity of both nitrogen and helium in the phase change from liquid to gas shown in Fig. 2, any boiling cryogen between the metallic structures will register a measurable change in capacitance.

The effectiveness of the technique is primarily due to the phase-change effect on the stray-capacitance, which is larger than that from thermal contraction or variations of permittivity with temperature in the liquid phase. The temperature rise and subsequent thermal expansion is negligible for heat loads smaller than needed to initiate boiling of cryogens. The size of the change in permittivity when boiling is larger than the cumulative shift from operating temperatures of 1.8–4.2 K for liquid helium and 60–77 K for liquid nitrogen to the boiling temperature in Fig. 2, although both the in-phase and phase-change shifts in permittivity are higher in the nitrogen system. This effect has been utilized for liquid cryogen level determination for decades but has only recently been investigated as a magnet diagnostic tool [7]–[9].

B. Implementation in High Temperature Superconducting Magnets

The stray-capacitance technique was tested in three magnets made with the HTS $Bi_2Sr_2CaCu_2O_{7+x}$ (Bi-2212) conductor. Like both Nb_3Sn and Nb-Ti, round-wire Bi-2212 can be made into Rutherford cables, the most common conductor geometry for building accelerator magnets. Simple double-pancake racetrack coils (RCs) have been used as a research and development program to investigate technology variants and demonstrate improvements in conductor performance [10], [11]. The canted cosine theta (CCT) magnet geometry is under investigation with continued research and development for Bi-2212 as a scalable solution to address the low yield-strength of Bi-2212 Rutherford cables [12], [13].

This article will compare these magnet systems in order to illustrate simple design considerations for implementing capacitance heat detection. The first question addressed by this study is whether this method can be useful to locate heat sources. In a simple RC magnet, RC6, we installed two identical capacitance probes symmetrically in the magnet to localize the response to pulses of a fixed heater located near one of the probes.

A second question addressed is how this method will work in practical magnet systems or other cold structures, as one of the strengths of this technique is the ease of implementing the system for existing magnet designs. With varying level of confinement of liquid cryogens, i.e., film interfaces with high surface tension or nearly enclosed volumes with tortuous or narrow openings, boiling cryogens can escape more or less easily, affecting the onset, saturation, and recovery of the capacitance change. The available structures for measuring stray-capacitance may extend over multiple possible heat sources or not cover the entire volume of interest, making it difficult to identify and isolate the causes of heat.

Quench detection utilizing stray-capacitance of the existing mechanical structures is compared between RC6 and two accelerator-type magnets. The first is a common coil dipole composed of two racetrack coils RC7 and RC8, abbreviated RC7n8, in which the external structure (iron yoke and loading pads) does not extend past the magnet to cover the terminal splices and is open enough to allow boiling gasses an easy path away from the magnet. The second is an outer layer from a CCT magnet, labeled CCT-OL, tested independently within a strong aluminum-alloy shell which does not cover the terminal splices but creates a narrow annulus for cryogen gases to escape the magnet. Whereas for single racetrack magnet testing, the

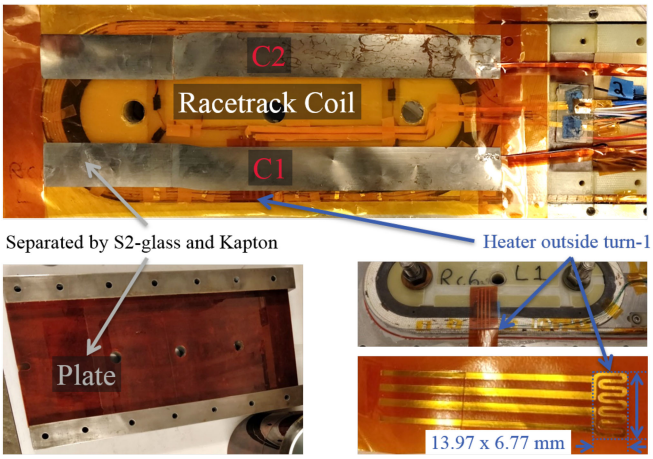

Fig. 3. Top: Capacitance sensors C_1 and C_2 installed above Bi-2212 RC6. Bottom-left: One of two Kapton and S2-glass isolated iron plates that constrain RC6. Middle-right: Heater location on outer turns of RC6. Bottom-right: Resistive four-wire heater. Figure reproduced from [6].

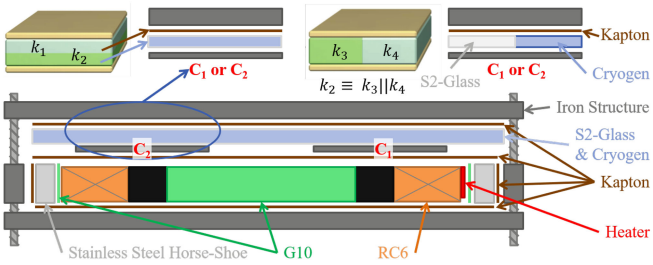

Fig. 4. 2-D cross section of the RC6 racetrack coil test structure with metal and dielectric structures forming capacitive elements labeled. A simple plate model is approximated by the iron, Kapton, S-2 glass, cryogen, and the sensors C_1 and C_2. Modified figure reproduced from [6].

iron structure provides tight cryogen containment and spans the entire windings as well as the terminal joints.

II. Single Racetrack Coil Measurements

A. Magnet and Measurement Description

The first magnet results are for the highest performing Bi-2212 Rutherford cable racetrack coil, RC6, made of Bi-2212 Rutherford cable for setting the stage for the measurement and researching the possibility of heat localization. These 30-cm long coils with a 15-cm straight section are wound around an Inconel structure and surrounded by a rectangular stainless steel enclosure, three sides making a horseshoe (HS) shaped piece and the last side filled by an "end-shoe" between the cable terminations. This is enclosed in iron consisting of two rectangular plates and bars shown in Fig. 3.

High sensitivity probes were formed between thin stainless quench-heater strips, located over straight sections of the superconducting windings, and the iron plate covering the entire magnet, acting as simple parallel plate capacitors with a porous dielectric separation. The two strips were separated from the plate by 0.2-mm woven S-2 glass and 0.13-mm thick Kapton shown in Figs. 3 and 4. The woven S-2 glass cloth acts as a spacer to allow a volume of cryogen to fill a portion of the space between the plate and the strips, C_1 and C_2. In general, pairs of stainless strip could be used, rather than a single plate and the structure, for better sensor isolation at the cost of increased thickness. Such probes can be easily insulated from the magnet with thin sheets of Kapton polyimide, as used here, or any nonporous insulator with high dielectric strength. This formed a flexible, low cross-sectional capacitance probe, with no low-frequency interference to the magnet circuit and a strong thermal link to any heat generated on either side of its overlap area. By placing multiple such probes, cryogenic systems or magnets can be subdivided into regions of interest.

The "U" shaped steel coil support, or HS, was also instrumented, as it has a very large parallel area overlap with the plate and can produce a sensitive response to any heat within the magnet system, as demonstrated in previous measurements [4]. As in the Fig. 1 schematic, with only two wires, the capacitance changes can be monitored in multiple ways without interference with the superconducting windings by connecting to the mandrel, the mechanical structure, or diagnostic sensors The three measured capacitors in RC6 testing were HS to the iron plate, C_1 to the iron plate, as well as C_2 to the iron plate.

The capacitance was measured for RC6 and RC7n8 using a ground-referenced Agilent E4980 A precision LCR meter at 100–300 kHz with a sampling time of 100 ms per measurement including settling and dead time. Using Numato Systems electro-mechanical relay multiplexing of three channels, the sampling time increased to 300 ms per channel and 1 s per measurement of all channels of RC6. The signals were routed using untwisted wires due to lack of feed-through channels, yet the noise level was manageable due to the fixed frequency signal used for measurement. For more sensitive applications, coaxial wires can be implemented from sensor to LCR meter, given dedicated feed-through channels. Before evaluating the quench response, a baseline measurement ac frequency sweep and capacitance response calibration with a controlled heat source like a film resistor was performed. Then the capacitance of multiple probes can be recorded in real time using a simple multiplexer. For transient events, the heat source can be located by comparing the response onset, peak amplitude, and recovery time (for transient sources) to determine the proximity of the hot spot to each sensor. The symmetry of probe locations and the primary heat paths must be analyzed when making location determinations. This requires some knowledge of the possible heat sources in the system such as developing resistance during a quench or accelerator beam losses.

B. Investigating Sensitivity and Localization

1) Heater Pulses: RC6 was equipped with an insulated ribbon heater, $1.4\,\mathrm{cm} \times 0.7\,\mathrm{cm}$, on the broad face of the outermost turn in the middle of the straight section adjacent to capacitance probe C_1. It was used for generating heat to initiate quenches in the coil windings and as a controlled energy source for evaluating the capacitance response in both liquid nitrogen and liquid helium.

Powering the heater for 6 s in liquid helium deposited 6 J of heat producing the change in capacitances shown in Fig. 5. The

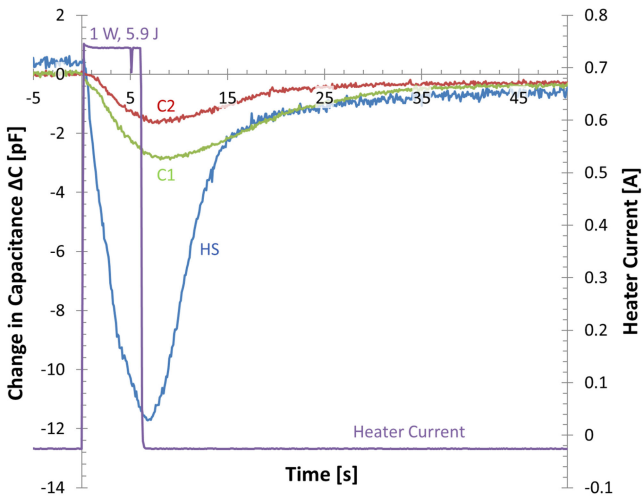

Fig. 5. Typical capacitance response from RC6, a single racetrack coil encased in a steel structure, for local strip sensors C_1 (green) and C_2 (red), and structural sensor HS (blue) to a heater current pulse (purple) in liquid helium. Figure reproduced from [6].

shape of the response is typical with a rapid rise during the heat pulse and a logarithmic return to the baseline. Fig. 6 summarizes the nonlinear heater pulse response with the peak change in capacitance as a function of the energy deposited in the heater for both cryogens. In liquid nitrogen, heat loads above 4 J are needed to produce a significant capacitance change. Above 25 J, the probe C_1 response flattens at a change of 6 pF. Conversely, the liquid helium response rises above the noise with only 0.1 J in the heater.

Fig. 5 shows that for constant heater pulses with no magnet transport current, we were able to observe a stronger and faster reaction from the capacitive probe, C_1, closer to the heater than from the probe further away, C_2. HS consistently had the strongest response and fastest recovery. The peak response was within a few seconds of the end of the heater pulse, but the half life for returning to baseline is closer to 5 s, reflecting a characteristic cooling time. The peak capacitance change is proportional to the deposited energy and begins to saturate at higher energies shown. This is consistent with all of the liquid between the sensor and plate being displaced with gas. No significant change in capacitance was observed for any sensor when pulsing the heater with the coil in nitrogen or helium gas.

2) High Current Quenches When Exceeding I_C: Spontaneous quenches were caused by exceeding the critical current of the symmetric, high-field, central windings above 8600 A. In contrast to the localized heater pulses, when a global superconducting transition occurred both C_1 and C_2 responded in kind. The structural sensor HS showed a more constant value when ramping the magnet far from the quench current, while C_1 and C_2 increased steadily with current. Despite the constant ramp rate, the capacitance change accelerates 5–10 s prior to energy extraction in Fig. 7, indicating more rapid heating prior to thermal runaway, as the rapid voltage rise only exceeded the 25 mV noise level for 10 ms before exceeding the quench detection threshold in Fig. 8. This is possible due to the high thermal margin of Bi-2212. The ≈1 s time required for multiplexing the three measurements does not appear detrimental to early capacitance detection, particularly for HTS-cable-wound magnets, where the stability is increased by strong current sharing.

The Bi-2212 Rutherford cable is so stable that the magnet was held at fixed currents of up to 90% of the quench limit with constant nonzero dissipative voltages and only a small decrease in capacitance for over 200 s without quenching. By ramping the magnet stepwise with plateaus of constant current, the Ohmic voltage could be measured at a much lower noise level shown in Fig. 9. This revealed a rise in the voltage with current analogous to the short sample power law I-V curve. When the magnet current was decreased to 70% of the quench limit, the capacitance change and voltages returned to their previous values, with a delay for the recovery of the capacitive signals.

3) Heater Induced Quench: Capacitance and Voltage Comparison: By running current pulses into the heater with the magnet at 90% of the quench current, the capacitive sensor response was compared to the magnet terminal voltage rise in Fig. 10. A deposited heater energy of 2–6 J was required to see dissipation in the voltage, while only 1 J was required to see a capacitive response. The sensor C_1 closer to the heater increased faster with higher deposited energy until an 8-J heater pulse. For subsequent pulses, it appears that the system may not have had enough time to cool sufficiently between heater pulses as the capacitive signals show a depressed baseline and a lower deposited energy of 6.4 J initiated a thermal runaway, requiring energy extraction to protect the magnet. The other possibility is that the higher power delivery of 6.1 W was sufficient to overcome cooling and generate a propagating normal zone. The voltage response was significant for the highest energy heater pulse with a multisecond recovery indicating the temperature was increased into the current sharing regime for some portion of the magnet windings.

C. Discussion—Modeling Local Sensors as Parallel Plate Capacitors With Series–Parallel Dielectrics

A simple plate capacitor model is formed of the support plate, Kapton, S-2 glass, and cryogen mixture, and either strip C_1 or C_2, as detailed in Fig. 4

$$\frac{1}{C_2} = \frac{1}{C_{\text{Kapton}}} + \frac{1}{C_s} \tag{1}$$

$$C_s = C_{\text{cryogen}} + C_{\text{S2glass}}. \tag{2}$$

The dielectric is assumed to have the fixed thickness Kapton layer in series with a parallel mixture of the liquid or gas cryogen and the S-2 glass cloth with an approximate 40% glass volume fraction

$$C_i = k_i \varepsilon_0 \frac{A_i}{d_i}. \tag{3}$$

The subscript for the dielectric constant k_i, the area A_i, and the distance between surfaces d_i refers to the three dielectric materials S2-glass, Kapton, and the liquid cryogen (either nitrogen or helium). Cryogenic temperature dielectric constants for each material were obtained from the literature [23]–[25]. Effects of

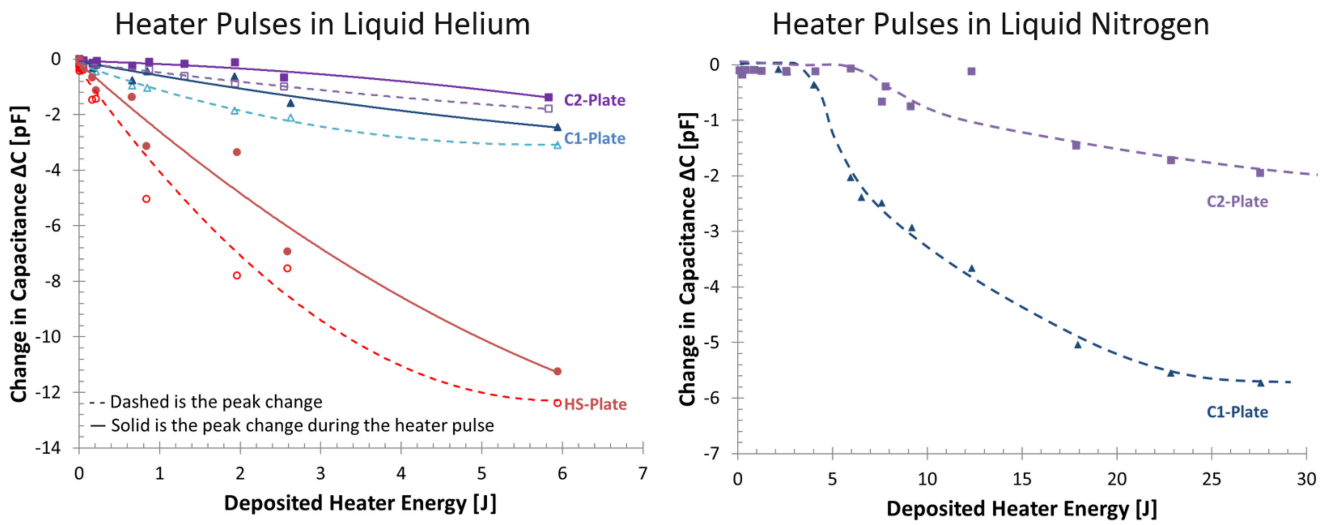

Fig. 6. Peak capacitance change registered for the RC6 sensors C_1, C_2, and HS to the iron plate structure following heater pulses in liquid helium (left) and nitrogen (right). Lines are a guide for the eye. Figure reproduced from [6].

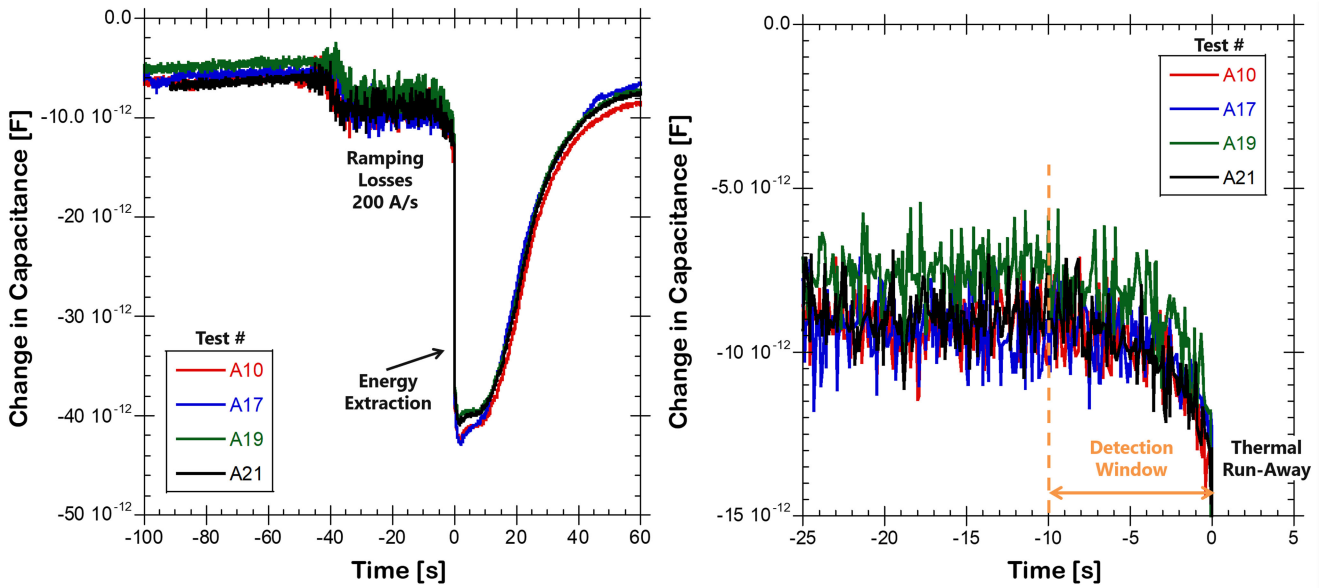

Fig. 7. Change in capacitance of the RC6 sensor HS to the iron plate structure for four separate quenches of the magnet RC6 with a rapid energy extraction at 0 s for the full time of the event (left) and 25 s before thermal run-away (right). Figure reproduced from [6].

thermal contraction on the material volumes were neglected. Despite multiple approximations, the calculated capacitance values, a total of 477 pF when liquid and 474 pF while gas, are within 20% of the measured values, 574 pF liquid and 566 pF gas, and the capacitance change between liquid and gas values are within a factor of three, a change in capacitance of 0.63% calculated versus 1.4% observed.

A straightforward explanation for the faster detection and slower recovery of C_1 than C_2 for heater pulses is that the cryogens boil near the heat source and travel out from the system through all available paths. This would explain the faster recovery of HS as it has the easiest cryogen exchange with the surrounding bath. The thermal source of the response explains the impressive sensitivity, shown in Fig. 10, to detect less than 1 J of heat in an electromagnetically noisy environment, in which voltage detection required 5–10 times as much heat input and noise reduction to see a clear response.

III. Common Coil Dipole Magnet Measurements

A. Magnet and Measurement Description

The common coil configuration is a block design, the simplest of which has two RCs with opposing currents generating a dipole field for the two apertures between the straight sections. The racetrack coils RC7 and RC8 are of a nearly identical design to RC6, except for a completely Inconel winding mandrel with a smaller diameter to accommodate 11 turns per layer instead of 6. To form a dipole, the RCs are separated by G-10 within an

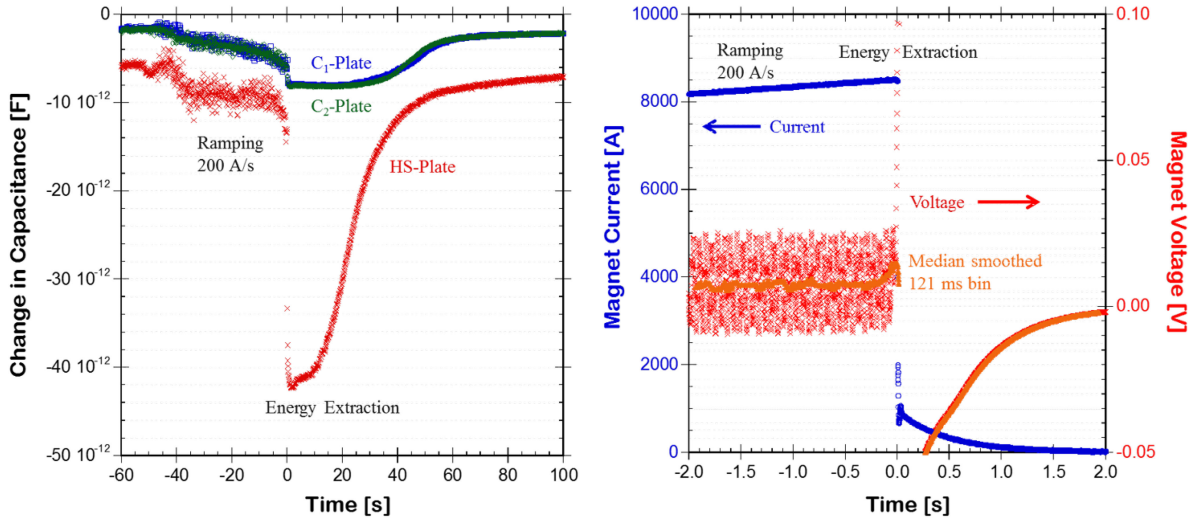

Fig. 8. Change in capacitance of the RC6 sensors C_1, C_2, and HS to the iron plate structure (left), and voltages and current of the magnet RC6 (right) during a 200 A s^{-1} ramp into quench with a rapid energy extraction at 0 s. Modified figure reproduced from [6].

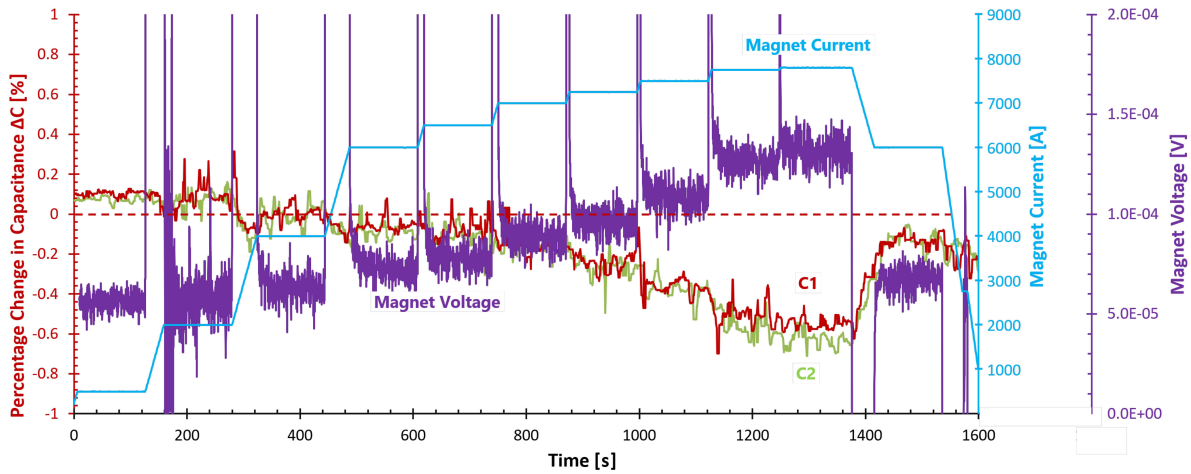

Fig. 9. RC6 magnet transport current, terminal voltage, and change in capacitance of the sensors C_1 and C_2 for a stepwise ramp up to 90% of the quench current and back down with no quench. Modified figure reproduced from [6].

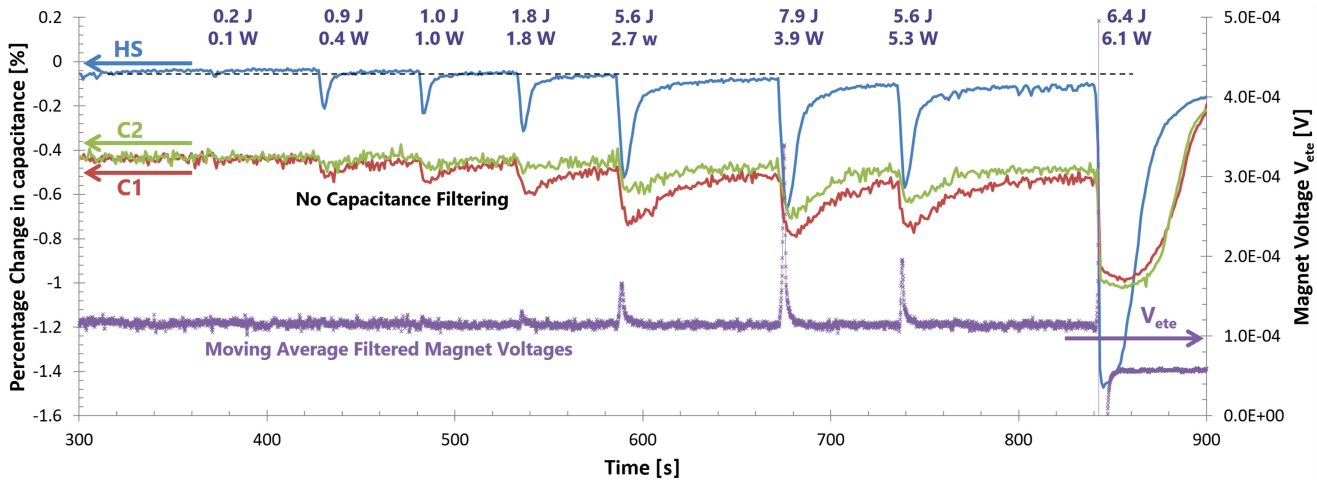

Fig. 10. Terminal voltage smoothed with a backward-looking moving average (averaged with earlier time data points) (purple), change in capacitance of the sensors C_1 (red), C_2(green), and HS (blue) for sequential heater pulses with a constant magnet current of 7600 A, 90% of the quench current, of the magnet RC6. Modified figure reproduced from [6].

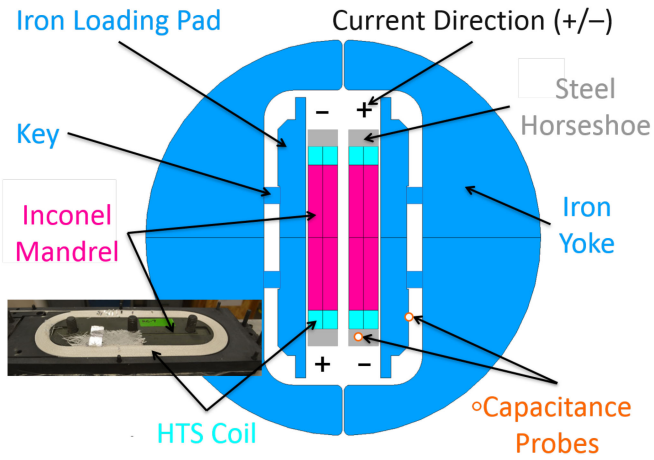

Fig. 11. Common coil dipole magnet composed of RC7 and RC8 with structures, current direction, and capacitance probe locations identified.

iron yoke inside an aluminum shell preloaded by a bladder-and-key process [26] as outlined in Fig. 11. One of the capacitance probe wires is connected at the steel HS around one of the coils and both HS are electrically shorted by the steel splice support connections. The other capacitance probe wire is connected to one of the iron loading pads and is electrically shorted to the iron yoke and other pressure pad through the loading keys, shims, and solid aluminum outer containment cylindrical shell (not shown). The thickness of dielectric layers was 0.13 mm of Mylar sheets for the common coil dipole.

B. Demonstrations in a Common Coil Dipole Magnet

For the tests of the common coil dipole RC7n8, the global stray-capacitance between the coil winding mandrels and the mechanical structures surrounding the magnets was monitored as if it were a quench detection signal. Typical results are shown in Fig. 12. The capacitance varied with current in the same fashion as the coil section voltages that are typically used for quench detection. The stray-capacitance signal had more noise than for the single racetrack structure. This noise is smoothed by taking a moving median with a bin size of 21 data points, with the effect demonstrated for the as measured and smoothed voltage data on the right in Fig. 12. The additional inductive portion of the voltage signal is clear when the current ramp is paused or changes direction. No significant difference in the stray-capacitance was observed between increasing and decreasing currents prior to quench. Additional capacitance change was observed when ramping up the current of RC7n8, a portion of which dissipated when the current was held steady at currents less than 5 kA. At higher currents, when the coil was within 5%–10% of the quench current, the signal held steady when the current stabilized.

C. Observing the Liquid Cryogen Fill Level From the Structural Stray-Capacitance

The stray-capacitance of the dipole, RC7n8, was monitored during the cool-down and cryogen fill to get a calibration of the decrease in capacitance with temperature and a long-term baseline before magnet operations. As a useful consequence of the phase-change mechanism of the change in stray-capacitance, the helium fill could be observed in Fig. 13 as an increase in capacitance after the magnet was at constant cold-mass temperature, as measured by a Cernox resistor. This is not unexpected, as capacitive cryogen level meters exist, but the clarity of the change from a dropping value during cool-down, to a rising capacitance while the level rises, with a stable stray-capacitance when the level is above the top of the structure was a surprising extra benefit for a diagnostic that requires no sensors to be installed. The temperature rises during the helium gas cool-down period relate to manual pressure control of the fill system. The stray-capacitance does not correlate directly with all of these more temporary temperature changes. The Cernox resistor is measuring only one part of the structure, while the stray-capacitance in gas depends upon the temperature of the dielectric and thermal contraction of multiple materials. The fill is more or less monotonic as the cold mass is at a much more uniform temperature once liquid can condensate and fill the volume.

IV. Canted Cosine Theta Outer Layer Coil Measurements

A. Magnet and Measurement Description

In the CCT configuration, the Rutherford cable follows machined grooves in an easily machinable aluminum-bronze alloy mandrel that has been found to be chemically compatible with the Bi-2212 reaction. A full CCT magnet consists of even numbered layers of tilted helices, with the current directions such that the axial field cancels and a "perfect" dipole component remains.

The mechanical layout, as well as images of the Bi-2212 windings and assembled structure of CCT-OL test, is detailed in Fig. 14. The capacitance probe wires were attached at the end of the aluminum bronze winding mandrel and to the end of the aluminum-alloy shell, separated by 0.2 mm of Kapton and G-10. For CCT-OL, capacitance was recorded with a GW Instek LCR-6020 at a maximum frequency of 20 kHz. A long averaging time was used during the system cool-down and warm-up for higher stability and precision, while the shortest averaging time was used during heater and quench events.

B. Demonstrations in a Canted Cosine Theta Coil

For the tests of the CCT-OL, the global stray-capacitance between the coil winding mandrels and the mechanical structures surrounding the magnets was monitored as if it were a quench detection signal. Typical results are shown in Fig. 15. Similar to RC7n8, the capacitance varied with current in the same fashion as the coil section voltages that are typically used for quench detection. The CCT-OL stray-capacitance signal also had more noise than for the single racetrack structure shown by the capacitance data in Fig. 15. For the CCT-OL magnet, the capacitance change remained stable when the current was held constant, with only a slow drift over time in Fig. 16. The

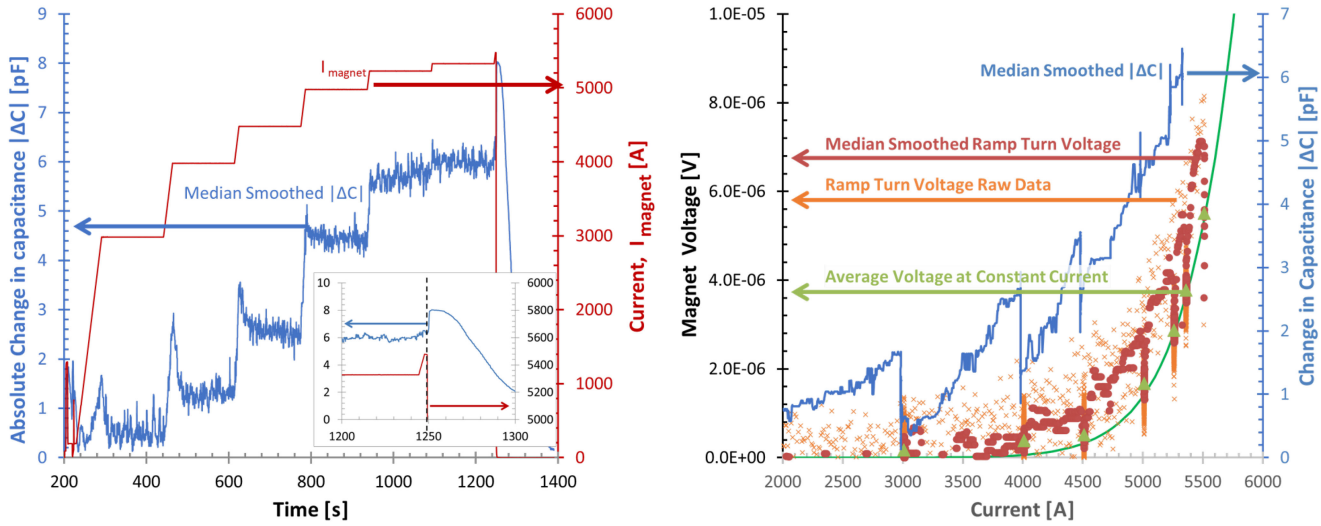

Fig. 12. Left: Change in capacitance (blue) and dipole current (red) for a ramp of the RC7n8 magnet into quench. Left inset zooms into the time around the quench. Right: Change in capacitance (blue), steady-state voltages (red and orange), and an I-V power-law fit (green) across the high field location of the ramp-turn between pancakes of RC7 when holding the current steady before the quench.

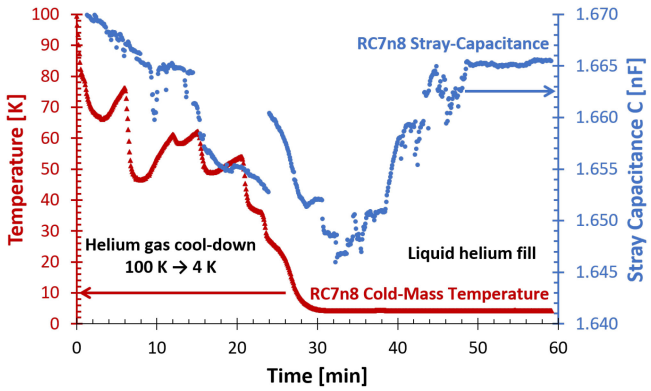

Fig. 13. Change in capacitance (blue circles) and cold-mass temperature (red triangles) of RC7n8 during a helium gas cool-down and liquid fill.

capacitance changed gradually with increasing current prior to energy extraction, after which the capacitance change peaked before returning to the baseline over a time period of minutes.

V. Discussion

A. Providing Reliable Diagnostics in Practical Magnet Tests

The boil-off mechanism for stray-capacitance quench detection is independent of the magnet geometry as the heat generated by the normal state transition will increase in power along with the power-law I-V response in Figs. 12 and 15. Unfortunately, it does not discriminate between heat from ramping losses, terminal or joint splices, flux-creep, and normal state resistance; so there is the possibility of false positive detection, in which the coil could recover if the current is held constant or reduced. This is especially true for the global stray-capacitance measured with structures where the splices are in thermal contact, like the HS to plate for the racetrack and winding mandrel to Al-shell for the CCT magnet. This is often the case in magnets because the terminal splices require mechanical reinforcement provided by extending the winding structure.

The global stray-capacitance approach is less than optimal because the locations with the availability of boiling liquid cryogen may be thermally insulated from the highest field regions most likely to quench that tend to be near the metallic mandrel and filled with epoxy. This may also change as the magnet trains and epoxy cracks provide unpredictable paths for liquid cryogens into the magnet. This is in contrast to the local parallel-plate approach described above, in which the cryogen is provided a location within the sensor which is thermally linked to a region of interest. The helium level effect is a beneficial result of the global approach, as the liquid cryogen filling the magnet is directly causing the response. If a local sensor is used, like a long narrow strip along the outside of the magnet, the helium level of the bath should produce a cleaner signal, but due to the heat capacity of the magnet cold mass, the global stray-capacitance may show a slower and more accurate fill as the entire structure cools.

The difference in stray-capacitance between ramping and steady current became smaller approaching quench in Fig. 12. This occurred as the static heat load exceeded 75% of the capacitance saturation reached during the quench, which displaced all of the liquid within the sensor. It appears that less recondensation is occurring when ramping is halted above 5 kA. This would be consistent with increased current sharing with the stabilizer and between filaments because of the higher resistive heat load and lower hysteretic component from the superconducting paths. Being able to diagnose when significant current sharing is beginning gives valuable information about the operating margins of the magnet, but if this is purely a matter of gas saturation, then it will be linked to the sensor configuration rather than the magnet operation. For example, in systems with less confinement of trapped volumes, the recondensation may occur up to higher heat loads, giving the system a more proportional response until all of the liquid is displaced. This is consistent with

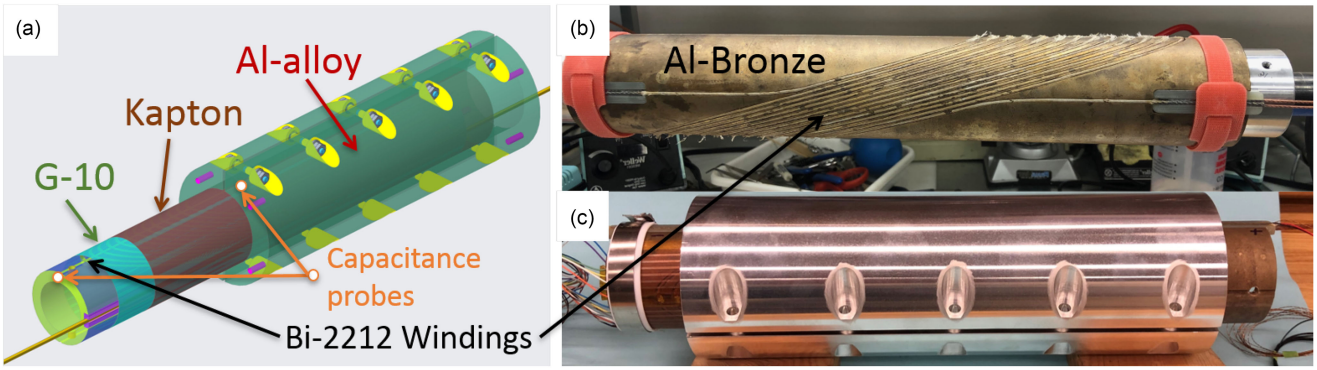

Fig. 14. (a) CCT-OL expanded assembly with the dielectric layers, metallic structures, and capacitance probe locations indicated. (b) Reacted Bi-2212 CCT-OL on the aluminum-bronze mandrel. (c) The fully assembled and instrumented CCT-OL coil.

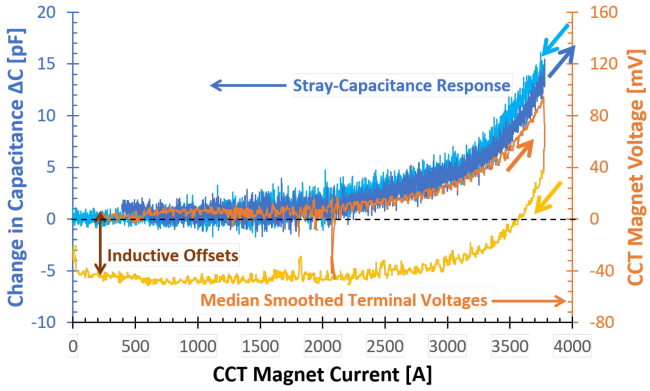

Fig. 15. Change in capacitance (blue) and median smoothed terminal voltage (orange/yellow) for a 9.4 A s^{-1} ramp of the CCT-OL magnet up to 93% of the quench current and back down without tripping the quench protection voltage criterion.

CCT-OL in Fig. 16, where there is no jump between ramping and steady-state operation.

B. Reducing Quench Validation Time With Capacitance Sensors and Section-Voltages

In using a capacitive sensor for quench detection, it would seem to be best as a secondary verification tool. Presently, to avoid false positive detection, a time delay is used to verify voltage threshold detection. This time could be reduced or eliminated if both capacitance threshold and voltage thresholds are surpassed. In the local quench spot case, the capacitance detection may be faster than the voltage rise as the heat will generate gas locally before a large conductor volume exhibits a voltage rise. In the case of a more global transition such as with overcurrents, the voltage may appear faster than the gas is generated at the sensor location. A suitable detection system could operate normally with an integration time for voltage signals, which could be bypassed if a capacitance condition is satisfied, either exceeding a threshold or a rate of change. A similar sort of verification control scheme could be used for heat load applications in conjunction with thermocouples or pressure values, as opposed to voltage measurements.

The results of these studies suggest several use cases. The most direct application from that studied here would be in an HTS magnet system such as the 32 T all superconducting magnet at the National High Magnetic Field Laboratory (NHMFL) [27]. This magnet consists of a series of stacked rare earth barium copper (REBCO) Oxide REBCO double pancakes of HTS tape conductor. As there are already heaters between the pancakes to protect the magnet in the case of a quench, a capacitive sensor could be formed using the heater as one half. The other half of the sensor could be measured from the magnet windings, thin isolated strips across the heater, a grid across the heaters, or even a second heater in parallel to the original by a relay until firing the heaters. Alternatively, the sensor could be formed of two polyimide insulated, stainless annuli inside or outside of the heater area so as to not affect the operation of the heaters. The advantage of the isolated strips or grid is that it gives the ability to further localize the heat generation with axial location (down to two pancakes) from which set of sensors, azimuthal location from which strip or grid section, and even possibly radial location if the grid can be subdivided and the data postprocessed to filter the noise from small capacitance sections. The downside is the number and complexity of the signal wiring rising quickly.

For a subdivided system, a set of capacitive bridges and multiplexing would be more economical. In normal operation, a parallel connection of the system could be measured to increase the signal-to-noise ratio and increase the sampling rate. Once an initial threshold has been exceeded, the system could multiplex regions or individual sensors during the event. This data could either be used for further verification or just for later analysis in order to localize the source of the heat as much as possible. This can be very useful for correlating with simulations and for improving operating procedures for avoiding undesired heat loads.

The joints between double pancake windings and at the current lead terminals of a system like the 32 T magnet would be another set of ideal locations for capacitive sensors. This could again be a single or double set of isolated strips the same width as the HTS tape covering the joint. Capacitance would be measured between the strip and the tape or the second strip. As the sensor would be in close thermal contact to the joint, there

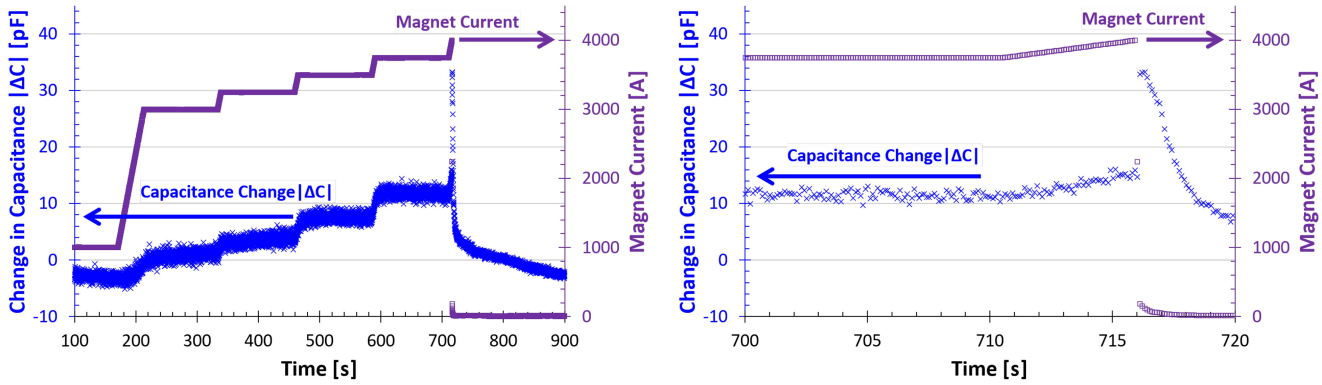

Fig. 16. Left: Change in capacitance (blue) of the magnet current (purple) for a stepwise ramp of the CCT-OL magnet, Right: Expanded time around tripping the quench protection at 4 kA.

would be little to no delay in the capacitance change. The benefit of the two isolated strips would be complete insulation from the high voltages present during a magnet quench, and reduction of other capacitive signals from the rest of the magnet windings. The dual-strip sensor would result in a simple easily installed and repairable monitor of the health of a joint independent of the superconducting and inductive properties that complicate the current voltage response.

VI. Conclusion

Stray-capacitance monitoring is an effective diagnostic tool, well-suited to highly stable HTS magnets with low normal zone propagation velocity. Specifically, we have shown the following. 1) With an array of distributed sensors, it can localize heat sources in a magnet. Local stray-capacitance probes were used to locate heat sources, including normal zones, in an HTS Bi-2212 RC. These parallel plate capacitors with a porous dielectric take up very little space in the magnet cross section but still generate clear responses. Heater pulses produced stronger and slower decaying changes in the closer capacitance probe. With the magnet under power, capacitance change was visible at less than 1 J heater energy, six times lower than it took to see a voltage rise. 2) It can even serve as an auxiliary quench detection method. Working with voltage taps, and it can improve quench detection integrity independent of magnet geometry, as demonstrated for a Bi-2212 RC, common-coil dipole, and a CCT coil. In RC6, the rapid change of capacitance was observed 10 s prior to thermal run-away and a voltage tripped energy extraction, making a clear case for using this method to reduce quench detection validation times, providing more time for active protection of HTS magnets. 3) It can be an *in situ* magnet liquid level sensor using only the magnet structural element as probes. Due to the liquid cryogen phase change mechanism, global stray-capacitance probes provided a monitor for the liquid level in the CCT magnet structure.

Acknowledgment

The authors would like to thank LBNL's Diego Arbelaez, Lucas Brouwer, and Laura Garcia Fajardo for their extensive work on the CCT program, NHMFL's Ernesto Bosque and Lamar English for heat treatments performed on RC coils and CCT coils, LBNL's Aurelio (Ray) Hafalia, Jim Swanson, Hugh Higley, Jordan Taylor, and Marcos Turqueti for experimental and technical support, Ian Pong (LBNL) and industry partners Yibing Huang with the Bruker OST LLC fabricated high performance Bi-2212 strands for HTS conductor and cabling, as well as Soren Prestemon (LBNL) and David Larbalestier (NHMFL) for leadership and operational support.

References

[1] S. Prestemon *et al.*, "The 2020 updated roadmaps for the U.S. magnet development program," Oct. 2020. [Online]. Available: https://science.osti.gov/-/media/hep/pdf/Reports/2020/USMDP-2020-Plan-Update-web.pdf?la=en&hash=CDF960B4B079A4182F024B159C87EF528B33B2C0

[2] M. Marchevsky, D. Arbelaez, and S. Prestemon, "Structural diagnostics of superconducting magnets using diffuse field ultrasound," *IEEE Trans. Appl. Supercond.*, vol. 30, no. 4, Jun. 2020, Art. no. 4703404.

[3] T. Strauss *et al.*, "Quench location in the LARP MQXFS1 prototype," *IEEE Trans. Appl. Supercond.*, vol. 28, no. 3, Apr. 2018, Art. no. 4001604.

[4] E. Ravaioli, M. Martchevskii, G. Sabbi, T. Shen, and K. Zhang, "Quench detection utilizing stray capacitances," *IEEE Trans. Appl. Supercond.*, vol. 28, no. 4, Jun. 2018, Art. no. 4702805.

[5] E. Ravaioli *et al.*, "A new quench detection method for HTS magnets: Stray-capacitance change monitoring," *Phys. Scripta*, vol. 95, no. 1, 2019, Art. no. 015002.

[6] D. S. Davis, "Quench protection of Bi_2 Sr_2CaCu_2 O_{8+x} high temperature superconducting magnets," Ph.D. dissertation, Florida State Univ., Tallahassee, FL, USA, 2019.

[7] I. V. Velichkov and V. M. Drobin, "Capacitive level meters for cryogenic liquids with continuous read-out," *Cryogenics*, vol. 30, no. 6, pp. 538–544, Jun. 1990.

[8] D. K. Hilton, J. S. Panek, M. R. Smith, and S. W. Van Sciver, "A capacitive liquid helium level sensor instrument," *Cryogenics*, vol. 39, no. 5, pp. 485–487, May 1999.

[9] K. Matsumoto, M. Sobue, K. Asamoto, Y. Nishimura, S. Abe, and T. Numazawa, "Capacitive level meter for liquid hydrogen," *Cryogenics*, vol. 51, no. 2, pp. 114–115, Feb. 2011.

[10] T. Shen *et al.*, "Stable, predictable and training-free operation of superconducting Bi-2212 Rutherford cable racetrack coils at the wire current density of 1000 A/mm^2," *Sci. Rep.*, vol. 9, no. 1, Dec. 2019, Art. no. 10170.

[11] T. Shen and L. G. Fajardo, "Superconducting accelerator magnets based on high-temperature superconducting Bi-2212 round wires," *Instruments*, vol. 4, no. 2, Jun. 2020, Art. no. 17.

[12] L. Garcia Fajardo *et al.*, "Fabrication of Bi-2212 canted-cosine-theta dipole prototypes," *IEEE Trans. Appl. Supercond.*, vol. 29, no. 5, Aug. 2019, Art. no. 4002005.

[13] L. G. Fajardo *et al.*, "First demonstration of high current canted-cosine-theta coils with Bi-2212 Rutherford cables," *Supercond. Sci. Technol.*, vol. 34, no. 2, Jan. 2021, Art. no. 024001.

[14] V. D. Arp, R. D. McCarty, and D. G. Friend, "Thermophysical properties of Helium-4 from 0.8 to 1500 K with pressures to 2000 MPa NIST," *Tech. Note (NIST TN) - 1334*, 1998. [Online].

Available: https://www.nist.gov/publications/thermophysical-properties-helium-4-08-1500-k-pressures-2000-mpa

[15] H. Brechna, W. A. Tuttle, R. G. Stewart, J. E. Jensen, and A. G. Prodell, "Selected cryogenic data notebook," Brookhaven Nat. Lab., Upton, NY, USA, Tech. Rep. TR-BNL 10200-R, 1980.

[16] A. Maryott and E. Smith, "Table of dielectric constants of pure liquids," in *National Bureau of Standards Circulation*, vol. 514. Washington, DC, USA: U.S. Government Printing Office, 1952.

[17] C. Grebenkemper and J. Hagen, "The dielectric constant of liquid helium," *Phys. Rev.*, vol. 80, no. 89, pp. 1129–1145.

[18] A. van Itterbeek and J. Spaepen, "Mesures sur la constante dielectique de quelques gaz non polaires (H2, D2, he, O2, et l'air) et CO entre la temperature ordinaire et 20 degAbs [measurements of the dielectric constants of several non-polar gases (H2, D2, he, O2, and air) and CO between ordinary temperature and 20 degAbs]," *Physica*, vol. 10, no. 3, pp. 173–84, 1932.

[19] L. Ebert and W. H. Keesom, "Voorloopige metingen van de dielectrische constante van vloeibare en vaste stikstof [preliminary measurements of the dielectric constants of liquid and solid nitrogen]," in *Proc. Commun. Phys. Lab.*, 1926, pp. 1188–1192.

[20] J. McLennan, R. Jacobsen, and J. Wilhelm, "Dielectric constants of liquefied gases," *Trans. Roy. Soc. Canada*, vol. 3, no. 24, pp. 37–46, 1930.

[21] R. Guillien, "Sur la variation de la constante dielectrique a la solidification des liquides homopolaires [regarding the change of the dielectric constant of homopolar liquids on solidification]," *Comput. Rend.*, vol. 207, pp. 393–395, 1938.

[22] C. Zahn, "The electric moment of CO_2, NH_3, SO_2," *Phys. Rev.*, vol. 27, pp. 455–459, 1926.

[23] J. Gerhold, "Properties of cryogenic insulants," *Cryogenics*, vol. 38, pp. 1063–1081, 1998.

[24] J. Clay and F. Van Der Maesen, "The absolute dielectric constant of gases at pressures of 0-80 atm. at 25 °C," *Physica*, vol. 15, no. 5, pp. 467–480, Jul. 1949.

[25] M. Wolfke and W. H. Keesom, "New measurements about the way in which the dielectric constant of liquid helium depends on the temperature," in *Proc. Commun. Leiden*, 1928, pp. 1924–1928.

[26] S. E. Bartlett *et al.*, "An R&D approach to the development of long Nb3Sn accelerator magnets using the key and bladder technology," *IEEE Trans. Appl. Supercond.*, vol. 15, no. 2, pp. 1136–1139, Jun. 2005.

[27] H. W. Weijers *et al.*, "Progress in the development and construction of a 32-T superconducting magnet," *IEEE Trans. Appl. Supercond.*, vol. 26, no. 4, Jun. 2016, Art. no. 4300807.